FULL PAPER

Self-Directed Localization of ZIF-8 Thin Film Formation by Conversion of ZnO Nanolayers

*Kira Khaletskaya, Stuart Turner, Min Tu, Suttipong Wannapaiboon, Andreas Schneemann, Robert Meyer, Alfred Ludwig, Gustaaf Van Tendeloo, and Roland A. Fischer**

Control of localized metal–organic framework (MOF) thin film formation is a challenge. Zeolitic imidazolate frameworks (ZIFs) are an important sub-class of MOFs based on transition metals and imidazolate linkers. Continuous coatings of intergrown ZIF crystals require high rates of heterogeneous nucleation. In this work, substrates coated with zinc oxide layers are used, obtained by atomic layer deposition (ALD) or by magnetron sputtering, to provide the Zn^{2+} ions required for nucleation and localized growth of ZIF-8 films ($[Zn(mim)_2]$; Hmim = 2-methylimidazolate). The obtained ZIF-8 films reveal the expected microporosity, as deduced from methanol adsorption studies using an environmentally controlled quartz crystal microbalance (QCM) and comparison with bulk ZIF-8 reference data. The concept is transferable to other MOFs, and is applied to the formation of $[Al(OH)(1,4\text{-ndc})]_n$ (ndc = naphtalenedicarboxylate) thin films derived from Al_2O_3 nanolayers.

1. Introduction

Zeolitic imidazolate frameworks (ZIFs) are a type of materials that combine the unique properties of both zeolites and metal-organic frameworks (MOFs), such as remarkably high surface areas, high grade of crystallinity, regular micropores as well as thermal and chemical stability.[1] The attractive potential of ZIFs as novel functional porous coordination network (PCNs) materials is displayed through their applications in gas storage,[2] separation,[3] chemical sensing[4] and catalysis.[5] The prototypical ZIF, $[Zn(mim)_2]$ (ZIF-8), is formed by combining a Zn^{2+} source and 2-methylimidazole (Hmim) in a suitable solvent and crystallizes in a sodalite-type structure.[6] The introduction of ZIF-8 as a thin film or membrane expands its utilization as sorbent and catalytic agent in powder form[7] towards further applications such as selective sensors for chemical vapors and gases[4a] or insulators in microelectronics.[8] In general, ZIF-8 membranes have been synthesized on different supports by in situ[9] and secondary growth methods.[10] However, significant problems such as poor nucleation, adhesion and intergrowth of ZIF crystals were discussed in the literature.[11] The main drawback for growing MOF and also ZIF films on non-functionalized supports is the low density of available nucleation sites in the form of functional groups such as OH groups from where the formation of MOF/ZIF crystals can proceed. Consequently, the direct solvothermal synthesis route is rather unfavorable for the growth of dense crystalline layers.[12] Therefore, the nucleation and thus the formation of homogeneous coatings of MOF/ZIF crystals on the substrate surface requires suitable functionalization in the form of self-assembled monolayers (SAMs)[12a,13] or preformed seeding coating[10f,14] of the supports (secondary growth). In contrast, an alternative fabrication strategy of MOF/ZIF thin films relies on the utilization of metal oxides nanostructures. This concept is based upon the idea that substrates coated with metal oxide (nano) layers or structures already provide the required metal ions for initiation of nucleation and sustainable growth of MOF crystals directly in close proximity to the substrate, without any other surface modifications.

The synthesis of MOFs directly from metal oxides has been shown to enable the use of inexpensive raw materials and to overcome the lack of control over the spatial localization of the crystallization which is a typical problem for other approaches.[15] It has been reported that ZnO or Zn surfaces can induce and favor the nucleation of ZIF-8 crystals with the possibility of the formation of ZIF-8 films.[16,17] Chen et al. reported the solvent-free synthesis of ZIF-8 by means of a direct reaction between ZnO and Hmim.[18] This direct acid-base approach was also applied by Román et al. for the synthesis of a family of ZIFs based on the reaction between ZnO/CoO/$Co(OH)_2$ and imidazolic ligands.[19] Carreon et al. demonstrated the synthesis of ZIF-8 from a solid-liquid interface

K. Khaletskaya, M. Tu, S. Wannapaibon, A. Schneemann, Prof. R. A. Fischer
Department of Inorganic Chemistry II
Ruhr-University-Bochum
Universitätsstr. 150
44780, Bochum, Germany
E-mail: ac2-office@rub.de
Dr. S. Turner, Prof. G. Van Tendeloo
Electron Microscopy for Materials Science (EMAT)
University of Antwerp
Groenenborgerlaan 171, B-2020, Antwerp, Belgium
R. Meyer, Prof. A. Ludwig
Chair for MEMS Materials and Materials Research Department
Ruhr-University-Bochum
Universitätsstr. 150, 44780, Bochum, Germany

DOI: 10.1002/adfm.201400559

via solution-mediated crystallization, whereas the ZIF crystals were grown from Zn foils in the presence of Hmim alcohol solutions.[17b] ZnO@ZIF-8 nanorods with a core-shell structure have also been synthesized from prefabricated ZnO nanorods in a reaction with Hmim.[20] Recently, the preparation of low-defect ZIF-8 tubular membranes, based on the modification of the substrate with ZnO sol and its activation prior to the membrane formation was reported by Zhang et al.[21]

In order to take full advantage of the functionality of the MOF/ZIF films, control over the crystal size, position and orientation is desirable. Various strategies to induce MOF nucleation in specific positions on different kinds of substrates have been reported and three different concepts can be identified.[22] Firstly, the MOF positioning (patterning) is controlled by use of an additive or specific agent.[23,24] Secondly, control is achieved by substrate chemistry or surface modification (e.g. localized electrochemistry, microcontact printing.[26] Thirdly, the MOF positioning is based on the application of an external field, e.g. magnetic patterning.[27] Despite this variety of procedures to position MOFs on surfaces, certain drawbacks still remain (e.g. poor nucleation and integration for device fabrication). Consequently, further advances are required to establish a versatile approach for localized MOF thin film formation, which is suitable for integration in device fabrication schemes.

A very powerful and widely established methodology for spatial positioning of materials (thin films, nanostructures), especially in microelectronics, is based on vapor phase deposition technologies. In particular, highly controlled deposition of nanoscale metal oxides is achieved by atomic layer deposition (ALD) or magnetron sputtering. Herein, we report on the combination of ALD and sputtering techniques with MOF thin film fabrication and demonstrate the self-directed localization of ZIF-8 thin film formation by conversion of ZnO nano layers (**Scheme 1**). The ZIF-8 coatings were obtained on silicon (Si/SiO_2) and on quartz crystal microbalance (QCM) substrates by wet-chemical, microwave-assisted conversion of pre-deposited ZnO layers derived from sputtering and ALD methods. The key feature of functional ZIF thin films (and MOFs or PCNs in general), for example for sensor applications, is porosity.[28] We therefore also applied our method to QCM-sensors coated with ZnO and probed the adsorption properties by nano gravimetry. To the best of our knowledge, this is the first report on localizing MOF thin film growth on substrates by conversion of ALD and sputter deposited metal oxides and including the characterization of the materials' microporosity based on Langmuir Type I isotherms.

2. Results and Discussion

2.1. Fabrication of ZIF-8 Films from ZnO Nanolayers

Firstly, the ZnO precursor films (~50–150 nm thickness) were obtained by atomic layer deposition (chemical thin film deposition method) and confocal radio frequency (RF) magnetron sputtering. These techniques have the highest potential for the fabrication of flat and uniform films with low stress and defect density as well as highly precise and variable thickness down to the low nano-meter range. For ALD of ZnO, diethylzinc (DEZ) was used as the organometallic Zn-source and deionized water was used as the O-source. The main characteristic of the ALD process is a sequential deposition procedure. ZnO is created here as a result of a surface chemical reaction. The X-ray diffraction (XRD) characterization of ALD-ZnO (47 nm) shows weak and broadened reflexes indexed as (100), (002) and (101), which match in both position and relative intensities with the hexagonal (wurtzite) ZnO reference (Figure S1), indicating that the grown films are not textured. The poor crystallinity of the films is confirmed by selected-area electron diffraction (SAED) analysis, showing only weak diffraction rings (Figure S2). According to these results, the ALD films are predominantly composed of randomly oriented ZnO nanocrystals, possibly imbedded in or associated with an amorphous ZnO matrix (which is typical for ALD-ZnO). Radio frequency magnetron sputtering (Ar) using a microcrystalline ZnO target yields the PVD-ZnO films. The corresponding XRD pattern (Figure S1) of a typical film (113 nm) deposited on a Si/SiO_2 substrate shows a similar pattern to the ALD-ZnO, except for an intense reflex at 34.5° 2Θ, which corresponds to diffraction from the (002) ZnO plane. The observed (002) preferential orientation is due to the typical growth of ZnO crystals in the form of long hexagonal rods along the c-axis, resulting in columnar grains that are perpendicular to the substrate. The SAED data (Figure S2) are complementary to the XRD data and confirm the pronounced crystallinity (more intense diffraction rings) of the sputtered ZnO with respect to the ALD-ZnO.

The ZnO thin films deposited on Si or QCM substrates were used as a sacrificial surface to deliver the Zn^{2+} ions for

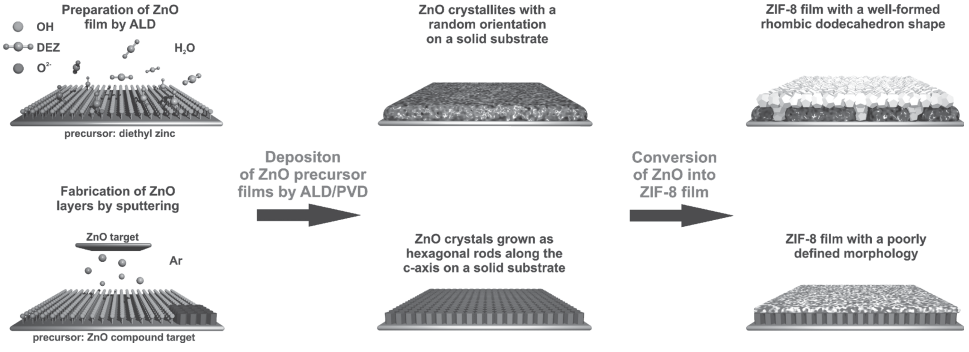

Scheme 1. Schematic illustration of the synthesis of ZIF-8 films from ZnO precursor films deposited on solid substrates.

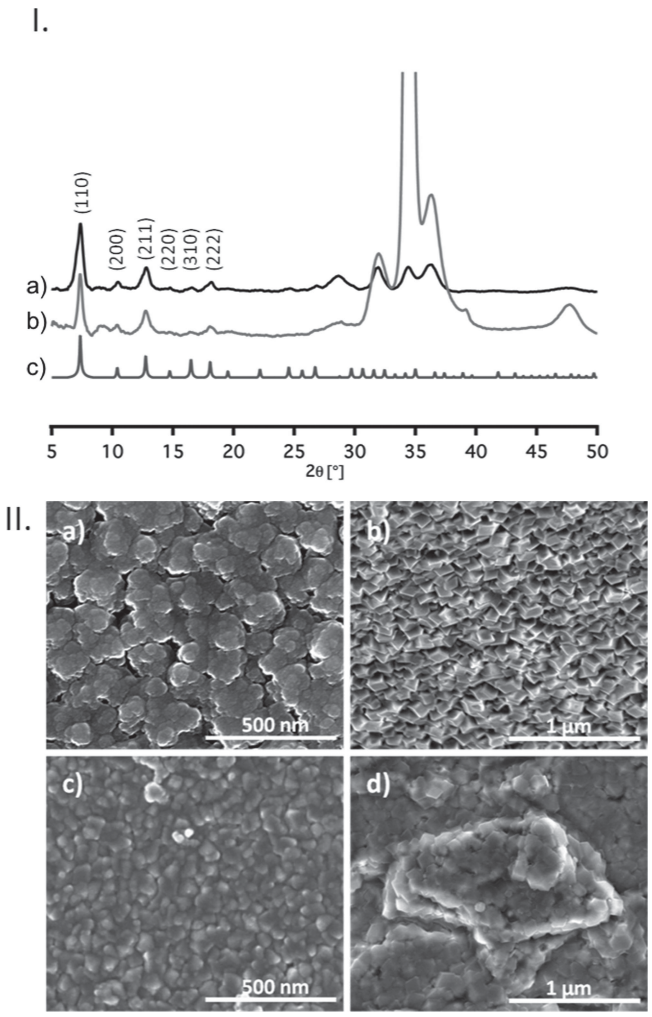

Figure 1. Phase composition and surface morphology of the ZIF-8/ZnO samples. (I, *left*) XRD patterns of ZIF-8 films obtained from ALD (a) and sputtered ZnO (b) compared with a calculated pattern of the bulk material (c). (II, *right*) SEM images of (a) ZIF-8 derived from sputtered ZnO on a Si substrate, (b) ZIF-8 derived from ALD-ZnO on a Si substrate, (c) ZIF-8 derived from sputtered ZnO on QCM sensor and (d) ZIF-8 derived from ALD-ZnO on QCM sensor.

initiation and support of ZIF-8 growth. The successful transformation from the ZnO film to the ZIF-8 film was carried out by immersion of the ZnO-coated substrates into the mixed solvent medium of *N,N*-dimethylformamide (DMF) and H_2O followed by a microwave-assisted treatment with 2-methylimidazole (linker component) at 80 °C for 1 h. The XRD patterns of the resulting coatings are shown in **Figure 1**(I) and reveal the successful formation of ZIF-8 in both cases. The main reflexes at 7.5° (110), 10.4° (200) and 12.8° (211) in 2Θ match well with the simulated pattern of the bulk material, based on Crystallographic Information File (CIF) reported by Yaghi et al.[6a] No significant difference in crystallinity is observed between the ZIF-8 films grown from either ALD or sputtered ZnO. The qualitative evaluation of the comparably weak intensities and line widths point to small (nano sized) randomly oriented ZIF-8 crystallites. The intense reflections in the range of 30–40 2Θ stem from the remaining ZnO coating and indicate that only a fraction of the ZnO film was converted to ZIF-8.

Generally, ZnO can easily be dissolved to release Zn^{2+} ions in acidic or basic aqueous solutions.[29] The key of the formation mechanism of intergrown ZIF-8 films is the role of the organic linker 2-methylimidazole, that acts both as an etching agent to dissolve ZnO films in order to provide Zn^{2+} ions and as a ligand for the coordination of Zn^{2+} ions to form ZIF-8. The linker creates homogeneous nucleation sites for the growth of a dense ZIF-8 film right on the substrate surface. The mechanism can only work when there is the right balance between the dissolution rate and coordination rate of Zn^{2+} ions. As reported previously, the dissolution of ZnO is too fast in H_2O and too slow in DMF.[30] Therefore, the ZIF-8 films were successfully synthesized in a mixed DMF/H_2O solvent. The reaction temperature and reaction time are further crucial factors which influence the success of the film formation. Dense, continuous and intergrown ZIF-8 films (Figure 1(II) and section 2.2. below) are synthesized at 80 °C after 1 h of microwave irradiation. An increase of the reaction time influences the amount of dissolved ZnO only in the case of ALD-ZnO, i.e. the remaining ZnO coating exhibits more areas in which the ZnO material appears to be almost fully converted to ZIF-8 (Figure S3). Figure 1(II) shows intergrown polycrystalline ZIF-8 layers with crystal sizes of ~50 nm on the top of Si and QCM substrates. The SEM images of the sputtered ZnO and the ALD-ZnO films before the partial conversion into the corresponding ZIF-8 films are presented in Figure S4. The crystal morphology of sputtered ZnO (a,c) and ALD-ZnO (b,d) clearly differs from each other. In the case of sputtered ZnO, the formed ZIF-8 structures are larger, due to the larger size of the ZnO particles obtained by the sputtering process, and the characteristic shape of ZIF-8 cannot be observed. In contrast, ZIF-8 films grown from the ALD-ZnO display a typical faceted shape of well-formed ZIF-8 crystals, which can be attributed to the fact that the formation of ZIF-8 films from a less dense, predominantly nanocrystalline ZnO precursor material is more effective due to the faster dissolution and conversion of the metal oxide. In general, SEM characterization proves the formation of dense, uniform and homogeneous ZIF-8 films on Si and QCM substrates in both cases. It can be concluded that nucleation and growth of the nanocrystals are both restricted to the location of ZnO precursor films.

2.2. Transmission Electron Microscopy (TEM) Characterization of ZIF-8 Films

Focused ion beam (FIB) milling is a suitable technique to prepare both cross-section and plan-view specimens from the grown ZIF-8 layers, in order to estimate the ZnO conversion progress and the thickness of the resulting ZIF-8 films. The TEM images in Figure S5 show cross-sectional views of the various layers in each sample. Bright-contrast ZIF-8 crystals can be seen on the top of the unconverted ZnO layer, which is deposited on a Si substrate. A thick Pt layer was deposited on top of the material for its protection prior to the milling procedure. The Pt signal is detected by energy dispersive X-ray elemental mapping (STEM-EDX). and represented in Figure S7.

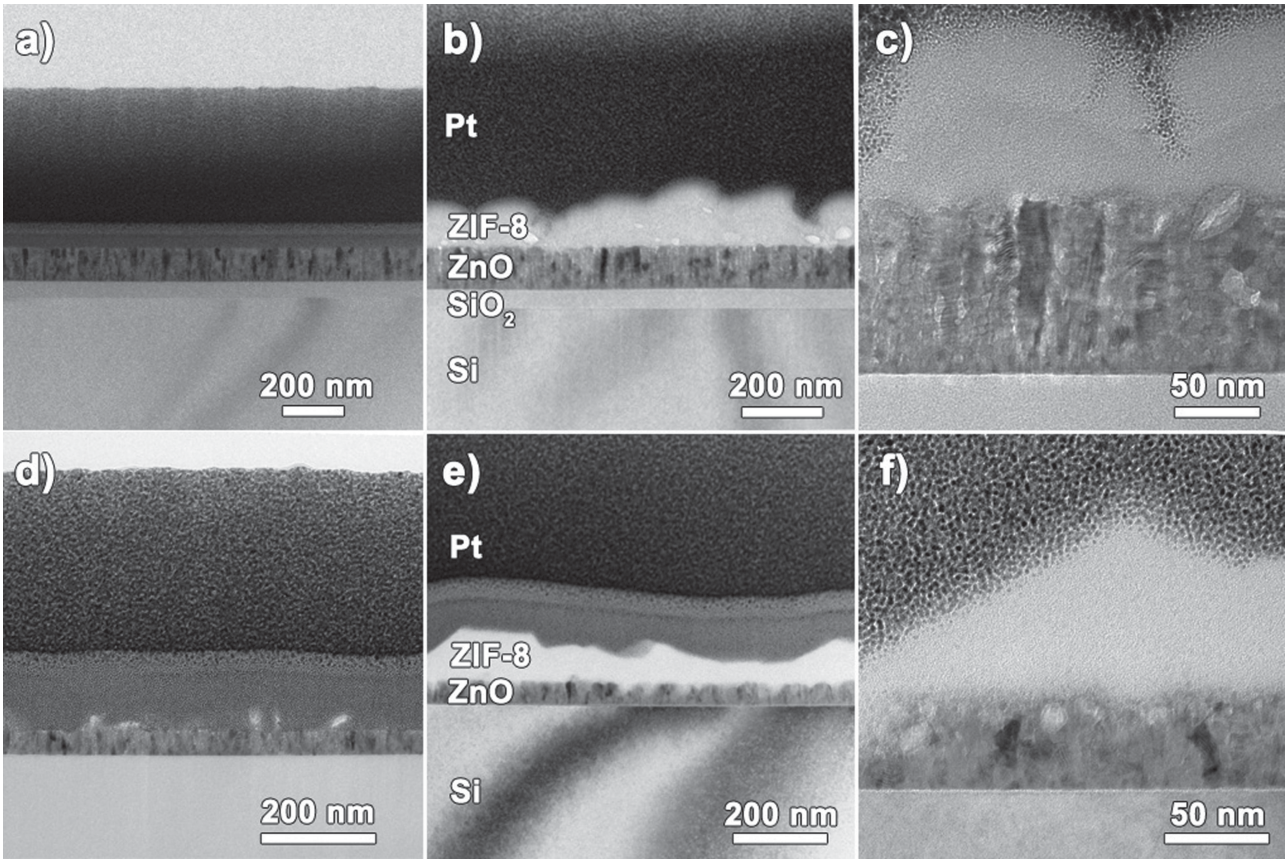

Figure 2. Microstructure of the grown ZIF-8 nano films. Bright-field TEM images of cross-sectional ZIF-8/ZnO samples on Si/SiO_2 substrates prepared by Focused Ion Beam (FIB), all samples are covered with a Pt layer of several hundreds of nms (see experimental part): (a) sputtered ZnO of 113 nm thickness, (b-c) ZIF-8 film (~80 ± 10 nm) grown from sputtered ZnO (c, magnification of image b); (d) ALD-ZnO of 47 nm thickness; (e-f) and ZIF-8 film (~95 ± 10 nm) grown from ALD-ZnO (f, magnification of image e). The microstructure of the ZIF-8/ZnO attached to the Si/SiO_2 substrate is nicely seen in images c and f: the bright contrast regions are the porous ZIF-8 films.

The FIB-prepared cross-sectional views in **Figure 2**a and d show uniform, polycrystalline ZnO precursor films. The sputtered layer in 2a exhibits a typical columnar growth perpendicular to the substrate. The initial thicknesses of the sputtered and ALD-ZnO films are 113 and 47 nm. During the microwave synthesis, ZnO layers of several nm thicknesses are dissolved and the resulting liberated Zn^{2+} ions coordinate to the linker and form the ZIF-8 coating.

In order to understand the coherence between the amount of the dissolved ZnO and the formed ZIF-8 nanocrystals, the density ratio $\gamma = \rho(\text{ZIF-8})/\rho(\text{ZnO})$ is introduced. For the estimation of the density of the thin film it was assumed that the reported density value for bulk ZIF-8 is also valid for thin films of the same type of material. The densities (ρ) of the ALD[31a] and sputtered ZnO are 4.47 g cm^{-3} and 5.61 g cm^{-3} and the theoretical density of crystalline ZIF-8[31b,c] is 0.95 g cm^{-3} giving $\gamma = 21.2$ and 16.9, respectively. The factors can be used for the estimation of the resulting ZIF-8 film thickness. If 1 nm of ALD-ZnO is dissolved by the linker, 21.2 nm of ZIF-8 film should be formed. In case of sputtered ZnO, 16.9 nm of ZIF-8 should be produced. The intergrown ZIF-8 crystals can be seen on top of the unconverted ZnO layers and the thickness of the films is 70–87 nm in case of the sputtered ZnO precursor and 85–106 nm in case of the ALD-ZnO film. Consequently, 4.1–5.1 nm of sputtered ZnO and 4–5 nm of ALD-ZnO precursor film have been consumed, which is in good agreement with the TEM results. Figure S6 shows a FIB-prepared TEM plan-view sample of well-formed ZIF-8 crystals grown from ALD- ZnO, and gives an additional insight into the conversion procedure. Generally, the thickness of the precursor film doesn't significantly change after the conversion procedure. This can be explained by a volumetric expansion of ZnO during transformation because of a significant increase in molar volume. The residual, partially transformed ZnO acts as a bridging layer between the substrate and the ZIF-8 nanocrystals providing an excellent substrate adhesion for the nanocrystals. Notably however, the precursor film cannot be fully converted due to the very fast formation of the first ZIF-8 crystals, which block the ZnO surface and its further dissolution through the organic linker. Consequently, only very thin (less than 10 nm) ZnO films are likely to be fully converted into corresponding ZIF films. Our examples qualitatively show the possibility of the conversion of ultrathin precursor films, enabling the precise control of the location of materials and opening further applications in field of the miniaturized devices.[32]

Scanning transmission electron microscopy–electron energy loss spectroscopy (STEM-EELS) and energy dispersive

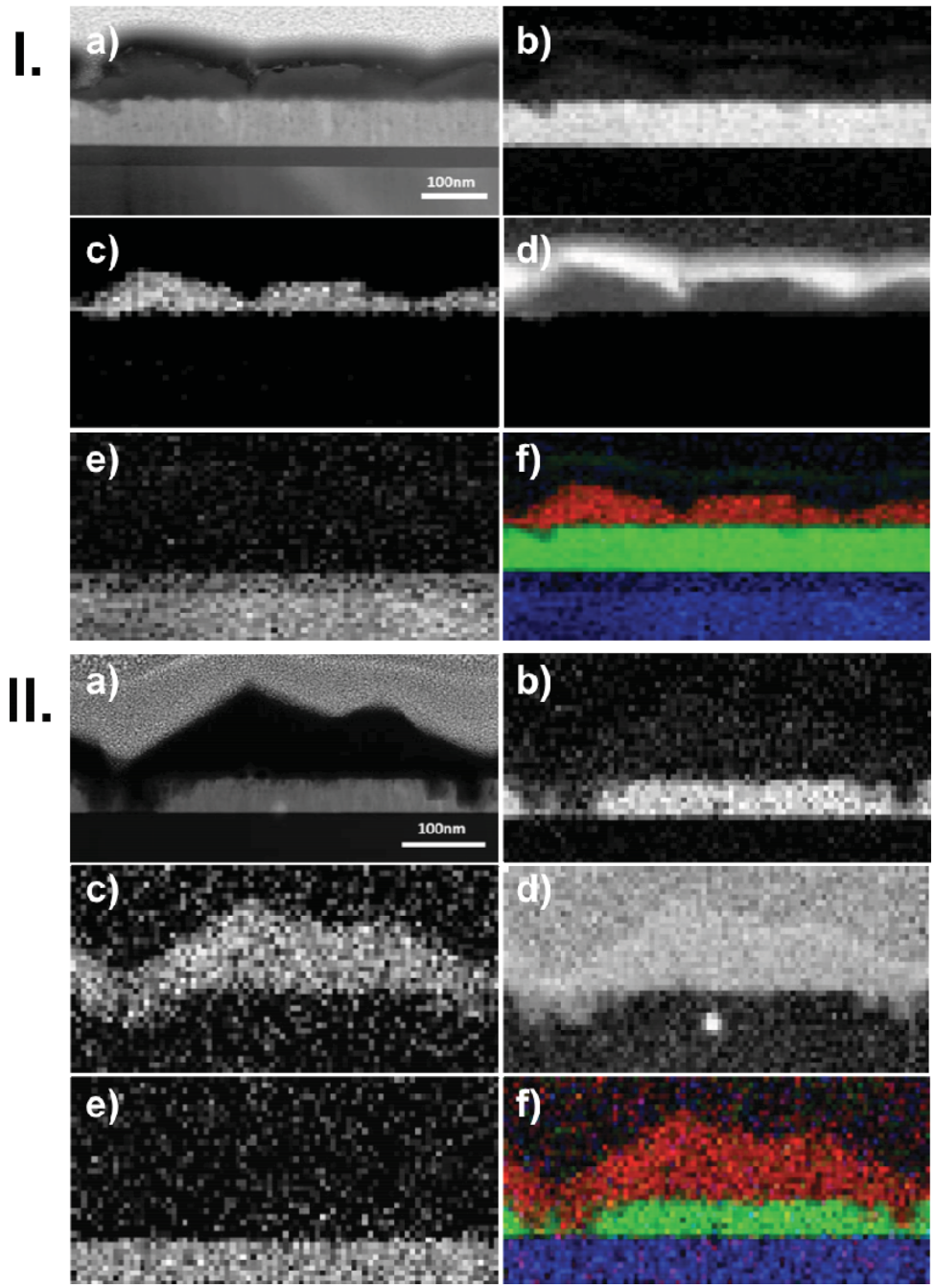

Figure 3. Elemental composition (mapping) by STEM-EELS. ZIF-8 films grown from sputtered ZnO (I, *above*) and grown from ALD-ZnO (II, *below*). Dark-Field image (a) and elemental maps of Zn (b), N (c), C (d) and Si (e). The RGB color maps in (f) display the merging of the elemental maps of N (red), Zn (green) and Si (blue). The localization of the N signals together with Zn and C clearly identify the region of ZIF-8 formation.

X-ray elemental mapping (STEM-EDX) were carried out to identify the elemental composition of the nanocrystals (**Figure 3** and Figure S7). Both methods display signals corresponding to the nitrogen in the ZIF-8 structure, which again supports the formation of ZIF-8 films. The RGB color models (Figure 3f) composed of the N, Zn and Si elemental maps illustrate the merging of these elements and clearly show the position of the ZIF-8 films on the top of the remaining ZnO.

2.3. Porosity Investigations of ZIF-8 Films via QCM

As mentioned above, the self-directed localization approach can also be applied to the synthesis of ZIF-8 films directly on the surface of QCM sensor substrates. The required low temperature (80 °C) and short reaction time (1 h) for the successful conversion of ZnO allow to avoid damage to the QCM sensors, which can be caused by high temperatures and long microwave treatments, and to investigate the methanol adsorption

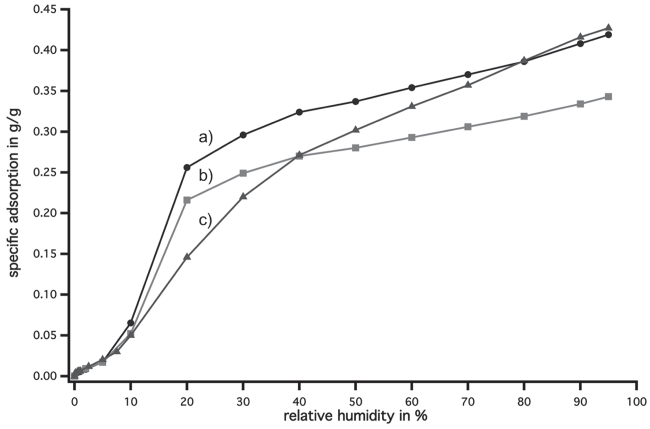

Figure 4. Microporosity of the ZIF-8 nano films. Methanol adsorption isotherms of two samples of ZIF-8 films grown from sputtered ZnO ((a) and (b)) measured at 298 K via QCM and comparison with a reference powder sample of microcrystalline ZIF-8 (c) deposited on the QCM sensor substrate by drop casting (see Experimental Section). The data show a similar behavior of the three samples reaching a specific saturation uptake [$g_{Methanol}/g_{ZIF\text{-}8}$] of 0.42 (a) and 0.32 (b) respectively. The good quality of the ZIF-8 nano films is indicated by their saturation uptakes being similar to the reference sample (c).

properties of the formed ZIF-8 films by the environment-controlled QCM technique at 298 K. To the best of our knowledge, this is the first report that MOFs/ZIFs nano films have been grown from a prefabricated metal oxide on the surface of a QCM sensor and have had their porosity properties investigated. Prior to the adsorption measurements (**Figure 4**) the samples were dried and activated as described in the experimental part. Methanol adsorption isotherms of ZIF-8 nano films ((a) and (b)) display a very similar over-all shape to the reference sample (c), clearly revealing the micro porosity of the films. The isotherm shape of the ZIF-8 nano films is slightly different from the Langmuir type I isotherms for N_2 adsorption of bulk ZIF-8 as previously reported, however they nicely match with the reported shape of the methanol adsorption isotherm of bulk ZIF-8.[34] To compare the saturation uptake of ZIF-8 films with the reference ZIF-8 material, three isotherms were measured simultaneously in a six-channel environmentally controlled QCM chamber. First, we compare two samples of ZIF-8 nano films, derived from sputtered ZnO obtained from two sources ((a) trace, ZnO on QCM substrate obtained from q-sense company (Sweden); (b) trace, ZnO on QCM fabricated by ourselves). The one ZIF-8 (a) exhibits only a slightly higher saturation uptake of 0.42 g/g at $P/P_0 = 95\%$ in comparison to the other ZIF-8 where a maximum loading of 0.32 g/g was reached. From these data adsorbed amounts of methanol molecules per Zn atom (3.0 and 2.3, respectively) are calculated. The values are in a good accordance with the reported uptake of 2.7 for the bulk ZIF-8 reference[34] and our own ZIF-8 powder sample (obtained from bulk ZnO, see Experimental Section) measured by QCM (c). The solvent-accessible volume (SAV) for the ZIF-8 nano films ((a) and (b)) was also calculated from the saturation uptakes (48.8% and 37.2%) and compared to the SAV value (50.4%)[33] of a ZIF-8 bulk reference material synthesized from $Zn(NO_3)_2{*}6H_2O$.[6] The slight but significant difference in the saturation uptakes of the ZIF-8 nano films is a clear indication that the crystallinity of ZIF-8 grown from non oriented sputtered ZnO (obtained from q-sense company, XRD in Figure S1) is higher than of ZIF-8 film fabricated from more crystalline and preferentially c-axis oriented sputtered ZnO obtained by ourselves.

2.4. Fabrication of $[Al(OH)(1,4\text{-ndc})]_n$ Thin Films from Al_2O_3 Nano Layers

The self-directed localization approach for the controlled MOFs/ZIFs growth on different substrates was extended to the fabrication of $[Al(OH)(1,4\text{-ndc})]_n$ films from amorphous aluminum oxide layers pre-deposited (by ALD) on Si. Recently, Furukawa's group showed the localized synthesis of this framework on the surface of gold nanorods[15b] which is achieved by coordination replication of alumina to Al-based MOF whereat the kinetic coupling between the dissolution of alumina and the crystallization of $[Al(OH)(1,4\text{-ndc})]_n$ allowed for the precise localization of MOF nucleation on the targeted environment.[15a] Using 1,4-naphthalenedicarboxylic acid H_2(1,4-ndc) as the etching agent and the coordination linker, we were able to convert an amorphous Al_2O_3 precursor layer into a corresponding $[Al(OH)(1,4\text{-ndc})]_n$ dense homogeneous film (Figure S8).

3. Conclusions

We have demonstrated a fast and effective self-directed localization strategy for the fabrication of dense and homogeneous films of ZIF-8 and $[Al(OH)(1,4\text{-ndc})]_n$ based on pre-deposited ZnO and Al_2O_3 nano layers. ALD and sputtering methods are employed to deposit ZnO on Si and QCM substrates which act as the sacrificial templates for the growth of the uniform and crystalline ZIF/MOF thin films. The demonstrated conversion of ultra thin precursor films into highly crystalline porous materials will open new possibilities in the fields of microelectronics and miniaturized devices.[35] The porosity of the ZIF-8 films obtained by spacial localization of the Zn^{2+} source on a solid support was investigated for the first time via the QCM technique. ALD offers ultra precise and high aspect ratio metal oxide positioning not only on flat substrates but also employing complex architectures and coating of internal surfaces of meso or macrostructured monoliths. The well established ALD technology platform, including organometallic and metal-organic precursor chemistry for metal oxide materials and special variants of ALD processes (thermal, photo- and plasma-assisted, etc.), together with lateral structuring methods (e.g. photolithography) suggest great potential for integration of MOF thin films and nanostructures into devices.

4. Experimental Section

Materials: All reagents and solvents were commercially available and used without further purification. 2-methylimidazole (99%), 1,4-naphthalenedicarboxylic acid and ZnO nanopowder were purchased from Aldrich Chemicals (Germany). Dimethylformamide was obtained by Fischer Chemicals (Germany). Chloroform was delivered by VWR International (Germany). In all experiments deionized water was used.

Sputter Deposition of ZnO: ZnO thin films were deposited by confocal radio frequency (RF) magnetron sputtering using an AJA ATC2200-V sputter system, equipped with a 4" ZnO compound target (Williams Advanced Materials, purity 99.9%). The depositions (RF Power: 100 W) were performed at room temperature and a sputter gas pressure of 1.33 Pa with an Ar flow of 40 sccm. The base pressure was better than $2.3*10^{-5}$ Pa for all samples. The substrates were rotated with 40 rpm, to achieve homogeneous thicknesses. Quartz crystal micro balance substrates (gold coated) and photolithographically structured Si/SiO_2 substrates were both mounted onto a 4" Si/SiO_2 wafers and ZnO thin films were deposited by sputtering as described above. In addition, QCM substrates coated with sputtered ZnO (150 nm) were obtained from q-sense company for comparison.

Atomic Layer Deposition (ALD) of ZnO: Atomic layer deposition (ALD) of ZnO films was performed at the Plasma Materials Processing (PMP) group of Applied Physics Department, Technical University Eindhoven, Netherlands. ZnO films were deposited on Si (4" wafers) using an open load Oxford instruments OpAL reactor at 100 °C. Diethyl zinc [DEZ, $Zn(C_2H_5)_2$] and deionized water (DI H_2O) vapor were used as precursors for the deposition of ZnO films. The dosing and purging times in one ZnO cycle were DEZ (50 ms)/purge (5 s)/DI H_2O vapor (20 ms)/purge (6 s) with a total of 247 ALD cycles (thickness ~50 nm). The base pressure was 1 mTorr and typical operating pressures were 100–1000 mTorr. Unfortunately, we could not obtain good quality ALD-ZnO nano films on (gold coated) QCM substrates.

Formation of ZIF-8 Nanofilm on ZnO-Coated Si/SiO_2 Substrates: The formation of ZIF-8 from ZnO (either derived by ALD or by sputtering) deposited on Si/SiO_2 was performed in a microwave reactor in a big excess of the organic linker. In a typical experiment, 2-methylimidazole (0.2 g) was added in a microwave reaction vessel (10 mL) containing a mixed solvent DMF/H_2O (6 mL). After a 5 min sonication a small piece of Si substrate coated with ALD (47 nm) or sputtered (113 nm) ZnO was added to the reaction mixture. The microwave synthesis was carried out for 1 h under stirring at 80 °C. After the reaction, the samples ZIF-8/ZnO@QCM were washed with DMF and H_2O several times and dried under ambient conditions.

Formation of ZIF-8 Film on ZnO-Coated QCM Sensors: Hmim (0.5 g) was sonicated with of DMF/H_2O solvent (16 mL). Then, QCM substrates coated with sputtered ZnO (150 nm, obtained by q-sense company; 113 nm obtained by ourselves) were added to a sonicated mixture in a microwave vessel (80 mL). The mixture was left to react under microwave irradiation for 1 h at 80 °C under stirring. The samples ZIF-8/ZnO@QCM were washed with water and DMF and dried under ambient conditions.

Synthesis of ZIF-8 Bulk Material: ZnO nanopowder (0.0204 g) was mixed with Hmim (0.1650 g) and put in the microwave reaction vessel (10 mL) containing the mixed solvent DMF/H_2O (6 mL). After a short sonication (several min), the mixture was heated at 80 °C for 1 h under stirring. The resulting material was washed with DMF and mixed with chloroform to exchange the DMF molecules.

Activation Procedure of ZIF-8 Films Prior to the Adsorption Measurements: The activation process was performed in two steps. Firstly, the QCM substrates coated with ZIF-8 nanofilms and the ZIF-8 reference powder sample were soaked in pure $CHCl_3$ for 1 h at 40 °C to exchange the DMF molecules. Then, the solvent was changed to the fresh one and this procedure was repeated several times. After the solvent exchange, a suspension of the reference ZIF-8 powder in $CHCl_3$ was dropped onto the QCM substrate and left at ambient conditions to evaporate the solvent. During the additional pretreatment the substrates were heated at 70 °C for 2 h in He stream inside the QCM chamber.

Methanol Adsorption Isotherms: The methanol adsorption properties of ZIF-8 nano films grown from sputtered ZnO on the QCM substrates and the reference bulk ZIF-8 powder material deposited on the QCM material were investigated by an environment controlled BEL JAPAN QCM instrument. Further details are given in the Supporting Information.

Formation of $[Al(OH)(1,4\text{-ndc})]_n$ Film on Si Substrate: A small piece of Al_2O_3@Si was added in a microwave vessel (10 mL) containing water and H_2(1,4-ndc) (200 mg). Some drops of nitric acid in H_2O were added to the mixture to adjust the pH value to 2. The mixture was stirred several minutes before heating to 180 °C for 1 h in the microwave. After cooling down, the material was washed with DMF and H_2O to remove the residual linker and dried under ambient conditions. The microstructural characterization data are given in the supporting information.

Supporting Information

Supporting Information is available from the Wiley Online Library or from the author.

Acknowledgements

The authors would like to thank Dr. Harish Parala from Ruhr University of Bochum, Prof. Leskela from University of Helsinki, Prof. W. M. M. Kessels and the PMP group at the Department of Applied Physics of Eindhoven University of Technology for providing the ALD grown ZnO samples used in this study and S. Van De Broeck from EMAT for the preparation of TEM samples by FIB milling. K. Khaletskaya gratefully acknowledges financial supports by the European Union under the Framework 7 program under a contract for an Integrated Infrastructure Initiative (Reference No.312483 ESTEEM2) and by the Research Department Interfacial Systems Chemistry (IFSC), Ruhr University Bochum. S.T. acknowledges the fund for scientific research Flanders (FWO) for financial support under the form of post-doctoral fellowship. The microscope used for this study was partially funded by the Hercules Foundation of the Flemish Government.

Received: February 18, 2014
Revised: March 17, 2014
Published online: May 7, 2014

[1] a) H. Hayashi, A. P. Cote, H. Furukawa, M. O'Keeffe, O. M. Yaghi, *Nat. Mater.* **2007**, *6*, 501; b) R. Banerjee, A. Phan, B. Wang, C. Knobler, H. Furukawa, M. O'Keeffe, O. M. Yaghi, *Science* **2008**, *319*, 939; c) B. Wang, A. P. Cote, H. Furukawa, M. O'Keeffe, O. M. Yaghi, *Nature* **2008**, *453*, 207; d) W. Morris, C. J. Doonan, H. Furukawa, R. Banerjee, O. M. Yaghi, *J. Am. Chem. Soc.* **2008**, *130*, 12626; e) R. Banerjee, H. Furukawa, D. Britt, C. Knobler, M. O'Keeffe, O. M. Yaghi, *J. Am. Chem. Soc.* **2009**, *131*, 3875; f) A. Phan, C. J. Doonan, F. J. Uribe-Romo, C. B. Knobler, M. O'Keeffe, O. M. Yaghi, *Acc. Chem. Res.* **2010**, *43*, 58.

[2] a) H. Wu, W. Zhou, T. J. Yildirim, *J. Am. Chem. Soc.* **2007**, *129*, 5314; b) L. J. Murray, M. Dinca, J. R. Long, *Chem. Soc. Rev.* **2009**, *38*, 1294; c) S. Q. Ma, H. C. Zhou, *Chem. Commun.* **2010**, *46*, 44.

[3] a) H. Bux, C. Chmelik, J. M. van Baten, R. Krishna, J. Caro, *Adv. Mater.* **2010**, *22*, 4741; b) Y. Li, F. Liang, H. Bux, W. Yang, J. Caro, *J. Membr. Sci.* **2010**, *354*, 48; c) Y. Liu, E. Hu, E. A. Khan, Z. J. Lai, *J. Membr. Sci.* **2010**, *353*, 36; d) M. C. McCarthy, V. Varela-Guerrero, G. V. Barnett, H.-K. Jeong, *Langmuir* **2010**, *26*, 14636.

[4] a) G. Lu, J. T. Hupp, *J. Am. Chem. Soc.* **2010**, *132*, 7832; b) S. Liu, Z. Xiang, Z. Hu, X. Zheng, D. J. Cao, *J. Mater. Chem.* **2011**, *21*, 6649.

[5] a) H. L. Jiang, B. Liu, T. Akita, M. Haruta, H. Sakurai, Q. Xu, *J. Am. Chem. Soc.* **2009**, *131*, 11302; b) C. Chizallet, S. Lazare, D. Bazer-Bachi, F. Bonnier, V. Lecocq, E. Soyer, A. Quoineaud, N. Bats, *J. Am. Chem. Soc.* **2010**, *132*, 12365; c) U. P. N. Tran, K. K. A. Le, N. T. S. Phan, *ACS Catal* **2011**, *1*, 120.

[6] a) K. S. Park, Z. Ni, A. P. Cote, J. Y. Choi, R. Huang, F. K. Uribe-Romo, H. K. Chae, M. O'Keeffe, O. M. Yaghi, *Proc. Natl. Acad. Sci. USA* **2006**, *103*, 10186; b) X. C. Huang, Y. Y. Lin, J. P. Zhang, X. M. Chen, *Angew. Chem. Int. Ed.* **2006**, *45*, 1557.

[7] a) Y. Wang, S. Jin, Q. Wang, G. Lu, J. Jiang, D. Zhu, *J. Chromatogr. A* **2013**, *1304*, 28; b) D. Esken, S. Turner, O. I. Lebedev, G. Van Tendeloo, R. A. Fischer, *Chem. Mater.* **2010**, *22*, 6393.

[8] S. Eslava, L. Zhang, S. Esconjauregui, J. Yang, K. Vanstreels, M. R. Baklanov, E. Saiz, *Chem. Mater.* **2013**, *25*, 27.

[9] a) Y. Liu, Z. Ng, E. A. Khan, H.-K. Jeong, C.-B. Ching, Z. Lai, *Microporous Mesoporous Mater.* **2009**, *118*, 296; b) Y. Liu, E. Hu, E. A. Khan, Z. P. Lai, *J. Membr. Sci.* **2010**, *353*, 36; c) G. Xu, J. Yao, K. Wang, L. He, P. A. Webley, C.-S. Chen, H. Wang, *J. Membr. Sci.* **2011**, *187*, 385; d) H. Bux, F. Liang, Y. S. Li, J. Cravillon, M. Wiebcke, J. Caro, *J. Am. Chem. Soc.* **2009**, *131*, 16000; e) M. Shah, H. T. Kwon, V. Tran, S. Sachdeva, H.-K. Jeong, *Microporous Mesoporous Mater.* **2013**, *165*, 63.

[10] a) S. R. Venna, M. A. Carreon, *J. Am. Chem. Soc.* **2010**, *132*, 76; b) Y. Pan, Z. P. Lai, *Chem. Commun.* **2011**, *47*, 10275; c) J. A. Bohrman, M. A. Carreon, *Chem. Commun.* **2012**, *48*, 5130; d) Y. S. Li, H. Bux, A. Feldhoff, G. Li, W. Yang, J. Caro, *Adv. Mater.* **2010**, *22*, 3322; e) F. Zhang, X. Zou, X. Gao, S. Fan, F. Sun, H. Ren, G. Zhu, *Adv. Funct. Mater.* **2012**, *22*, 3583; f) Y. S. Li, F. Liang, H. Bux, A. Feldhoff, W. Yang, J. Caro, *Angew. Chem. Int. Ed.* **2010**, *49*, 548.

[11] a) D. Zacher, O. Shekhah, C. Woll, R. A. Fischer, *Chem. Soc. Rev.* **2009**, *38*, 1418; b) A. Betard, R. A. Fischer, *Chem. Rev.* **2012**, *112*, 1055; c) D. Bradshaw, A. Garai, J. Huo, *Chem. Soc. Rev.* **2012**, *41*, 2344.

[12] a) S. Hermes, F. Schroder, R. Chelmowski, C. Woll, R. A. Fischer, *J. Am. Chem. Soc.* **2005**, *127*, 13744.

[13] a) M. O'Keeffe, M. Eddaoudi, H. Li, T. Reineke, O. M. Yaghi, *J. Solid State Chem.* **2000**, *152*, 3; b) A. Huang, H. Bux, F. Steinbach, J. Caro, *Angew. Chem. Int. Ed* **2010**, *49*, 4958.

[14] R. Ranjan, M. Tsapatsis, *Chem. Mater.* **2009**, *21*, 4920.

[15] a) J. Reboul, S. Furukawa, N. Horike, M. Tsotsalas, K. Hirai, H. Uehara, M. Kondo, N. Louvain, O. Sakata, S. Kitagawa, *Nature Mat.* **2012**, *11*, 717; b) K. Khaletskaya, J. Reboul, M. Meilikhov, M. Nakahama, S. Diring, M. Tsujimoto, S. Isoda, F. Kim, K. Kamei, R. A. Fischer, S. Kitagawa, S. Furukawa, *J. Am. Chem. Soc.* **2013**, *135*, 10998.

[16] a) Y. Hu, X. Dong, J. Nan, W. Jin, X. Ren, N. Xu, Y. M. Lee, *Chem. Commun.* **2011**, *47*, 737; b) W. Wang, X. Dong, J. Nan, W. Jin, Z. Hu, Y. Chen, J. Jiang, *Chem. Commun.* **2012**, *48*, 7022; c) X. Dong, K. Huang, S. Liu, R. Ren, W. Jin, Y. S. Lin, *J. Mater. Chem.* **2012**, *22*, 19222; d) X. Dong, Y. S. Lin, *Chem. Commun.* **2013**, *49*, 1196.

[17] a) M. Zhu, S. R. Venna, J. B. Jasinski, M. A. Carreon, *Chem. Mater.* **2011**, *23*, 3590; b) M. Zhu, J. B. Jasinski, M. A. Carreon, *J. Mater. Chem.* **2012**, *22*, 7684; c) Y. Yue, Z.-A. Qiao, X. Li, A. J. Binder, E. Formo, Z. Pan, C. Tian, Z. Bi, S. Dai, *Cryst. Growth Des.* **2013**, *13*, 1002; d) I. Stassen, N. Campagnol, J. Fransaer, P. Vereecken, D. De Vos, R. Ameloot, *CrystEngComm* **2013**, DOI: 10.1039/C3CE41025K.

[18] J. B. Lin, R. B. Lin, X. N. Cheng, J. P. Zhang, X. M. Chen, *Chem. Commun.* **2011**, *47*, 9185.

[19] M. Lanchas, D. Vallejo-Sánchez, G. Beobide, O. Castillo, A. T. Aguayo, A. Luque, P. Román, *Chem. Commun.* **2012**, *48*, 9930.

[20] W. Zhan, Q. Kuang, J. Zhou, X. J. Kong, Z. Xie, L. Zheng, *J. Am. Chem. Soc.* **2013**, *135*, 1926.

[21] X. Zhang, Y. Liu, L. Kong, H. Liu, J. Qiu, W. Han, L. T. Wenig, K. L. Yeung, W. Zhu, *J. Mater. Chem. A* **2013**, *1*, 10635.

[22] P. Falcaro, D. Buso, A. J. Hill, C. M. Doherty, *Adv. Mater.* **2012**, *24*, 3153.

[23] a) Y. S. Li, H. Bux, A. Feldhoff, G. L. Li, W. S. Yang, J. Caro, *Adv. Mater.* **2010**, *22*, 3322; b) D. Buso, A. J. Hill, T. Colson, H. J. Whitfield, A. Patelli, P. Scopece, C. M. Doherty, P. Falcaro, *Cryst. Growth. Des.* **2011**, *11*, 5268.

[24] a) O. Shekhah, H. Wang, T. Strunskus, P. Cyganic, D. Zacher, R. A. Fischer, C. Wöll, *Langmuir* **2007**, *23*, 7440; b) O. Shekhah, H. Wang, S. Kowarik, F. Schreiber, M. Paulus, M. tolan, C. Sternemann, F. Evers, D. Zacher, R. A. Fischer, C. Wöll, *J. Am. Chem. Soc.* **2007**, *129*, 15118; c) O. Shekhah, H. Wang, M. Paradinas, C. Ocal, B. Schüpbach, A. Terfort, D. Zacher, R. A. Fischer, C. Wöll, *Nat. Mater.* **2009**, *8*, 481.

[25] a) R. Ameloot, L. Stappers, J. Fransaer, L. Alaerts, B. F. Sels, D. E. De Vos, *Chem. Mater.* **2009**, *21*, 2580; b) R. Ameloot, L. Pandey, M. Van der Auweraer, L. Alaerts, B. F. Sels, D. E. De Vos, *Chem. Commun.* **2010**, *46*, 3735; c) R. Ameloot, E. Gobechiya, H. Uji-i, J. A. Martens, L. Alaerts, B. F. Sels, D. E. De Vos, *Adv. Mater.* **2010**, *22*, 2685.

[26] a) M. Cavallini, F. Biscarini, *Nano Lett.* **2003**, *3*, 1269; b) E. Bellido, S. Cardona-Serra, E. Coronado, D. Ruiz-Molina, *Chem. Comm.* **2011**, *47*, 5175; c) C. Carbonell, I. Imaz, D. Maspoch, *J. Am. Chem. Soc.* **2011**, *13*, 2144.

[27] a) M. R. Lohe, K. Gedrich, T. Freudenberg, E. Kockrick, T. Dellmann, S. Kaskel, *Chem. Commun.* **2011**, *47*, 3075; b) T. Loiseau, C. Mellot-Draznieks, H. Muguerra, G. Férey, M. Haouas, F. C. R. Taulelle, *Chimie* **2005**, *8*, 765; c) F. Ke, Y. P. Yuan, L. G. Qiu, Y. H. Shen, A. J. Xie, J. F. Zhu, X. Y. Tian, L. D. Zhang, *J. Mater. Chem.* **2011**, *21*, 3843.

[28] M. Meilikhov, S. Furukawa, K. Hirai, R. A. Fischer, S. Kitagawa, *Angew. Chem. Int. Ed.* **2012**, *52*, 341.

[29] a) Q. Kuang, T. Xu, Z. X. Xie, S. C. Lin, R. B. Huang, L. S. Zheng, *J. Mater. Chem.* **2009**, *19*, 1019; b) R. Remias, A. Kukovecz, M. Daranyi, G. Kozma, S. Varga, Z. Konya, I. Kiricsi, *Eur. J. Inorg. Chem.* **2009**, 3622.

[30] W. W. Zhan, Q. Kuang, J. Z. Zhou, X. J. Kong, Z. X. Xie, L. S. Zheng, *J. Am. Chem. Soc.* **2013**, *135*, 1926.

[31] a) K.-H. Lin, S.-J. Sun, S.-P. Ju, J.-Y. Tsai, H.-T. Chen, J.-Y. Hsieh, *J. Appl. Phys.* **2013**, *113*, 073512; b) Q. Song, S. K. Nataraj, M. V. Roussenova, J. C. Tan, D. J. Hughes, W. Li, P. Bourgoin, M. A. Alam, A. K. Cheetham, S. A. Al-Muhtasebd, E. Sivaniah, *Energy Environ. Sci.* **2012**, *5*, 8359; c) K. S. Park, Z. Ni, A. P. Coté, J. Y. Choi, R. Huang, F. J. Uribe- Romo, H. K. Chae, M. O'Keeffe, O. M. Yaghi, *Proc. Natl. Acad. Sci. USA* **2006**, *103*, 10186.

[32] D. M. Sun, M. Y. Timmermans, Y. Tian, A. G. Nasibulin, E. I. Kauppinen, S. Kishimotol, T. Mizutani, Y. Ohno, *Nat. Nanotechnol.* **2011**, *6*, 156.

[33] J. T. Hughes, T. D. Bennett, A. K. Cheetham, A. Navrotsky, *J. Am. Chem. Soc.* **2013**, *135*, 598.

[34] X.-C. Huang, Y.-Y. Lin, J.-P. Zhang, X.-M. Chen, *Angew. Chem. Int. Ed.* **2006**, *45*, 1557.

[35] A. Schwartzberg, V. Stavila, A. A. Talin, M. D. Allendorf, *Chem. Eur. J.* **2011**, *17*, 11372.